

# Modal locking between vocal fold oscillations and vocal tract acoustics

Tiina Murtola<sup>1,2)</sup>, Atte Aalto<sup>2,3)</sup>, Jarmo Malinen<sup>2)</sup>, Daniel Aalto<sup>4,5)</sup>, Martti Vainio<sup>4)</sup>

<sup>1)</sup>Dept. of Signal Processing and Acoustics, Aalto University, Finland

<sup>2)</sup>Dept. of Mathematics and Systems Analysis, Aalto University, Finland

<sup>3)</sup>Luxembourg Centre for Systems Biomedicine, University of Luxembourg, Luxembourg

<sup>4)</sup>Institute of Behavioural Sciences (SigMe group), University of Helsinki, Finland

<sup>5)</sup>Communication Sciences and Disorders, University of Alberta, Canada.

## 1 Summary

During voiced speech, vocal folds interact with the vocal tract acoustics. The resulting glottal source–resonator coupling has been observed using mathematical and physical models as well as in *in vivo* phonation. We propose a computational time-domain model of the full speech apparatus that contains a feedback mechanism from the vocal tract acoustics to the vocal fold oscillations. It is based on numerical solution of ordinary and partial differential equations defined on vocal tract geometries that have been obtained by magnetic resonance imaging. The model is used to simulate rising and falling pitch glides of [a, i] in the fundamental frequency ( $f_o$ ) interval [145 Hz, 315 Hz]. The interval contains the first vocal tract resonance  $f_{R1}$  and the first formant  $F_1$  of [i] as well as the fractions of the first resonance  $f_{R1}/5$ ,  $f_{R1}/4$ , and  $f_{R1}/3$  of [a]. The glide simulations reveal a locking pattern in the  $f_o$  trajectory approximately at  $f_{R1}$  of [i]. The resonance fractions of [a] produce perturbations in the pressure signal at the lips but no locking.

## 1 Introduction

The classical source–filter theory of vowel production assumes that the source (i.e., the vocal fold vibration) operates independently of the filter (i.e., the vocal tract, henceforth VT) whose resonances modulate the resulting sound [1, 2]. Even though this approach captures a wide range of phenomena in speech production, some observations remain unexplained by the source–filter model lacking feedback. The purpose of this article is to address some of these observations using computational modelling.

In this work, simulations where the fundamental frequency ( $f_o$ ) rises and falls over the range [145 Hz, 315 Hz] are considered for vowels [a] and [i]. Similar glides recorded from eleven female test subjects are treated in the companion article [3]. Such

glides are particularly interesting when the  $f_o$  range intersects an isolated acoustic resonance of the supra- or subglottal cavity. Since the lowest formant  $F_1$  usually lies high above  $f_o$  in adult male phonation, this situation is more typical in females and children when they are producing vowels with low  $F_1$  such as [i]. As reported in Section 5, simulations reveal (in addition to other observations) a characteristic locking behaviour of  $f_o$  at the VT acoustic resonance<sup>1</sup>  $f_{R1} \approx F_1$ .

This article has two equally important objectives. Firstly, we pursue better understanding of the time-domain dynamics of glottal pulse perturbations near  $f_{R1}$  of [i]. An acoustic and flow-mechanical model of the speech apparatus is a well-suited tool for this purpose. Secondly, we introduce and validate a computational model that meets these requirements. The proposed model has been originally designed to be a glottal source for a high-resolution 3D computational acoustics model of the VT which is being developed for medical purposes. There is also an emerging application for such models as a development platform of speech signal processing algorithms [5, 6, 7]. Since perturbations of  $f_o$  near  $F_1$  are a widely researched, yet quite multifaceted phenomenon, as discussed next, it is a good candidate for model validation experiments.

The simulations carried out in this article indicate special kinds of perturbations in vocal folds vibrations near a VT resonance. The mere existence of such perturbations is not surprising considering the wide range of existing literature. Since the seminal work of [8], a wide range of glottal source perturbation patterns related to acoustic loading has been investigated. Experiments were carried out in [9] on excised larynges mounted on a resonator to determine how glottal amplitude ratio changes with the subglottal resonator length. Physical models were used in [10] with a subglottal resonator to study phonation onsets and offsets, and in [11] with sub- and supraglottal resonators to study phonation onsets. The latter also considered

<sup>1</sup>The notation of [4] is used to differentiate resonances and formants though, of course, we expect  $f_{Rj} \approx F_j$  for  $j = 1, 2, \dots$

79 the dynamics of frequency jumps as the natural fre-  
 80 quency of their physical model was varied over time.  
 81 Similarly, a physical model of phonation with a tubu-  
 82 lar, variable length supraglottal resonator was studied  
 83 in [12, 13], and it was used to validate a flow-acoustic  
 84 model somewhat resembling the one proposed in this  
 85 article.

86 The source-filter interaction problem was ap-  
 87 proached in [14] using both reasoning based on  
 88 sub- and supraglottal impedances and a non-  
 89 computational flow model as well as computational  
 90 model comprising a multi-mass vocal fold model and  
 91 wave-reflection models of the subglottal and supra-  
 92 glottal systems. A two-mass model of vocal folds,  
 93 coupled with a variable-length resonator tube, was  
 94 used in [15], and pitch glides were simulated using a  
 95 four-mass model to analyse the interactions between  
 96 vocal register transitions and VT resonances in [16].

97 These works reveal a consistent picture of the ex-  
 98 istence of perturbations caused by resonant loads,  
 99 and this phenomenon has also been detected exper-  
 100 imentally in [17] using speech recordings, in [18] us-  
 101 ing simultaneous recordings of laryngeal endoscopy,  
 102 acoustics, aerodynamics, electroglottography, and ac-  
 103 celeration sensors, and in [19] using simultaneous  
 104 speech, electroglottography and accelerometer record-  
 105 ings combined with separate resonance estimation  
 106 measurements.

107 Although the existence of these perturbations has  
 108 been well reported, speech modelling studies have  
 109 given only limited attention to the time-domain dy-  
 110 namics of fundamental frequency glides where such  
 111 perturbations would be expected to occur. Of the  
 112 above mentioned studies, upward glides were simu-  
 113 lated in [11] by varying the natural frequency of their  
 114 physical model over time. Their small amplitude  
 115 oscillation model exhibited a frequency jump when  
 116 crossing the resonance of their downstream tube when  
 117 the acoustic coupling was sufficiently strong. Down-  
 118 ward glides were simulated in [14] followed by upward  
 119 glides by varying the parameters of a multi-mass vo-  
 120 cal fold model. Frequency jumps, subharmonics and  
 121 amplitude changes were observed in the regions where  
 122 load reactances were changing rapidly. Changes in the  
 123 rate of change of the fundamental frequency in these  
 124 regions can also be seen in their Figures 10-14. In [16]  
 125 upward glides were simulated followed by downward  
 126 glides by adjusting the tension parameter (i.e., de-  
 127 creasing masses and increasing stiffness parameters by  
 128 the same factor) in their four-mass vocal fold model.  
 129 They observed frequency jumps associated with reg-  
 130 ister changes, which in turn were shown to occur at  
 131 different frequencies depending on the VT load.

132 Some of the most popular approaches to modelling  
 133 phonation are based on the Kelly-Lochbaum VT [20]  
 134 or various transmission line analogues [21, 22, 23].  
 135 Contrary to these approaches, the proposed model  
 136 consists of (ordinary and partial) differential equa-

tions, conservation laws, and coupling equations. In  
 this modelling paradigm, the temporal and spatial  
 discretisation is conceptually and practically separ-  
 ated from the actual mathematical model of speech.  
 The computational model is simply a numerical solver  
 for the model equations, written in MATLAB environ-  
 ment. The modular design makes it easy to decou-  
 ple model components for assessing their significance  
 to simulated behaviour.<sup>2</sup> Since the generalised Web-  
 ster’s equation for the VT acoustics assumes intersec-  
 tional area functions as its geometric data, VT config-  
 urations from magnetic resonance imaging (MRI) can  
 be used without transcription to non-geometric model  
 parameters. Further advantages of speech modelling  
 with Webster’s equation have been explained in [25].

The proposed model is of low order: it aims at qual-  
 itatively realistic functionality, tunability by a low  
 number of parameters, and tractability of model com-  
 ponents, equations, and their relation to biophysics.  
 Similar functionality in higher precision can be ob-  
 tained using computational fluid dynamics with elas-  
 tic tissue boundaries. Such approaches aim to model  
 the speech apparatus as undivided whole [26], but the  
 computational cost is much higher compared to our  
 model or the models proposed in, e.g., [25] and [27].  
 Numerical efficiency is a key issue because some pa-  
 rameter values or their feasible ranges (in particular,  
 for hard-to-get physiological parameters) can only be  
 determined by trial and error, leading to a high num-  
 ber of required simulations as discussed in [30, Chap-  
 ter 4]. The proposed model is hence suitable for in-  
 vestigating speech phenomena where realistic model  
 output is only produced with a narrow range of con-  
 trol parameter values.

## 2 Phonation Model

### 2.1 Vocal Fold Mechanics

Voiced speech sounds originate from self-sustained  
 quasi-periodic oscillations of the vocal folds where the  
 closure of the aperture between the vocal folds, i.e.  
 the glottis, cuts off the airflow from lungs in a process  
 called phonation. A single period of the glottal flow  
 produced by phonation is known as a glottal pulse.

The main mechanism controlling the  $f_o$  of voiced  
 speech is contraction of the cricothyroid muscles  
 which leads to stretching the vocal folds and hence  
 increased stress. Secondary mechanisms of  $f_o$  control  
 include the vertical movement of larynx and changes  
 in the subglottal pressure through the control of res-  
 piratory muscles.

<sup>2</sup>Some economy of modelled features is desirable to prevent  
 “overfitting” while explaining experimental facts. Good mod-  
 elling practices in mathematical acoustics have been discussed  
 in [24, Chapter 8].

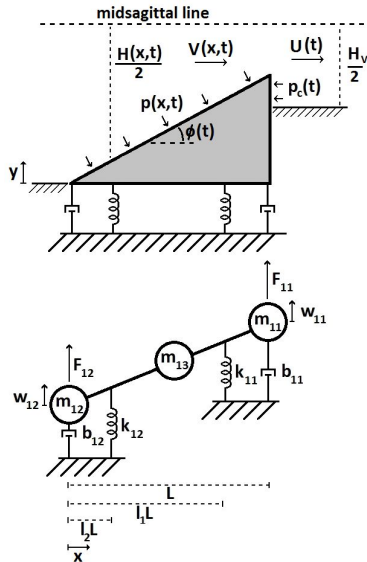


Figure 1: Top: The geometry of the glottis model with the trachea to the left and the vocal tract to the right. Bottom: Lumped-element representation of the lower vocal fold ( $j = 1$ ) with two degrees of freedom.

### 2.1.1 Equations of motion

The anatomic vocal fold configuration is idealised as a low-order mass-spring system with aerodynamic surfaces as shown in Figure 1. For previous uses and more details on this model, see [28, 29, 30] and [31]. Such lumped-element models have been used frequently (see, e.g., [13, 32, 33, 34, 35, 36] and the reviews [37, 38]) since the introduction of the classic two-mass model [8].

The radically simplified glottis geometry in Figure 1 (top) corresponds to the coronal section through the center of the vocal folds. Both  $f_o$  and the phonation type can be changed by adjusting parameter values [30, Section 4]. However, register shifts are not within the scope of this model.

The vocal fold model consists of two wedge-shaped moving elements whose distributed mass is reduced to three mass points which, for the  $j^{\text{th}}$  fold,  $j = 1, 2$ , are located so that  $m_{j1}$  is at  $x = L$ ,  $m_{j2}$  at  $x = 0$ , and  $m_{j3}$  at  $x = L/2$ . Here  $L$  denotes the thickness of the vocal fold structures. The masses are calculated so that the reduced system retains the mass, and static and inertial moments of a parabolic vocal fold shape (for details, see [31, p. 14]). Each vocal fold has two degrees of freedom:  $m_{j1}$  and  $m_{j2}$  can move in the  $y$ -direction. Although this causes some distortion to the shape of the wedges, the displacements in the  $x$ -direction are small enough that the effect is negligible. The elastic support of the vocal ligament is approximated by two springs at points  $x = l_1L$  and  $x = l_2L$ , and losses caused by internal resistance of the tissues

to movement and deformation is represented by two dampers at points  $x = 0$  and  $x = L$ .

The equations of motion for the vocal folds are

$$\begin{cases} M_1 \ddot{W}_1(t) + B_1 \dot{W}_1(t) + K_1 W_1(t) = F_1(t), \\ M_2 \ddot{W}_2(t) + B_2 \dot{W}_2(t) + K_2 W_2(t) = F_2(t), \end{cases} \quad t \in \mathbb{R}, \quad (1)$$

where  $W_j(t) = [w_{j1}(t) \ w_{j2}(t)]^T$  are the displacements of  $m_{j1}$  and  $m_{j2}$  in the  $y$ -direction as shown in Figure 1 (bottom). The load force pair  $F_j(t) = [F_{j1}(t) \ F_{j2}(t)]^T$  comprises acoustic pressure forces as well as aerodynamic pressure forces when the glottis is open (equation (9)) and collision forces when the glottis is closed (equation (5)). The mass, damping, and stiffness matrices  $M_j$ ,  $B_j$ , and  $K_j$ , respectively, in (1) are

$$M_j = \begin{bmatrix} m_{j1} + \frac{m_{j3}}{4} & \frac{m_{j3}}{4} \\ \frac{m_{j3}}{4} & m_{j2} + \frac{m_{j3}}{4} \end{bmatrix}, \quad B_j = \begin{bmatrix} b_{j1} & 0 \\ 0 & b_{j2} \end{bmatrix},$$

$$\text{and} \quad K_j = \sum_{i=1}^2 k_{ji} \begin{bmatrix} l_i^2 & l_i(1-l_i) \\ l_i(1-l_i) & (1-l_i)^2 \end{bmatrix}. \quad (2)$$

The entries of these matrices have been computed using Lagrangian mechanics. The damping matrices  $B_j$  are diagonal since the dampers are located at the end-points of the vocal folds. The model supports asymmetric vocal fold vibrations but for this work, symmetry of left and right vocal folds is imposed by using parameters  $M = M_j$ ,  $K = K_j$ , and  $B = B_j$ ,  $j = 1, 2$ , and by setting  $F(t) = F_2(t) = -F_1(t)$ . As a further simplification, tissue damping is assumed to be uniform everywhere, i.e.,  $b_i = \beta$  for  $i = 1, 2$ . The parameters in (2) as well as the load force components in (1) are illustrated in Figure 1.

The gap between the vocal folds is denoted by  $H(x, t)$ , and in the model geometry (Figure 1 (top))

$$H(x, t) = H_0(t) + \frac{x}{L} (H_L(t) - H_0(t)), \quad x \in [0, L], \quad (3)$$

where inferior glottal gap  $H_0(t) = H(0, t)$  and superior glottal gap  $H_L(t) = H(L, t)$  are related to (1) through

$$\begin{bmatrix} H_L(t) \\ H_0(t) \end{bmatrix} = W_2(t) - W_1(t) + \begin{bmatrix} g_L \\ g_0 \end{bmatrix}. \quad (4)$$

The rest gap parameters  $g_0$  and  $g_L$  correspond to the points  $x = 0$  and  $x = L$ , respectively.

### 2.1.2 Vocal fold collision

When the glottis is closed (i.e.,  $H_L(t) < 0$ ), there is no airflow between the vocal folds and hence no force arising from it affecting the vocal folds. There are, however, nonlinear spring forces with parameter  $k_H$ , accounting for the contact force of the vocal folds. They are accompanied by the acoustic counter pressure from the VT and subglottal tract (SGT), denoted

256 by  $p_c = p_c(t)$  in (15). Thus, the force pair for equation  
257 (1) during glottal closed phase is given by

$$F = F_H = \left[ \begin{array}{c} k_H |H_L|^{3/2} - A_{pc} p_c \\ A_{pc} p_c \end{array} \right], \quad \text{for } H_L < 0, \quad (5)$$

258 where the area  $A_{pc} = A_{pc}(t)$  is the nominal area on  
259 which  $p_c$  acts corrected with relative moment arms  
260 (see equation (16)).

261 This approach is related to the Hertz impact model  
262 that has been used similarly in [32] and [39]. When  
263 the glottis is open (i.e.,  $H_L(t) > 0$ ), the spring force  
264 in (5) is not enabled. Then the load terms in equa-  
265 tion (1) are given by  $F(t) = F_A(t)$  as introduced in  
266 equation (9) in terms of the aerodynamic forces from  
267 the glottal flow.

## 268 2.2 Glottal Flow Aerodynamics

269 The main component of the airflow within the speech  
270 apparatus, to which the acoustic component acts as  
271 a perturbation, is assumed to be incompressible and  
272 one-dimensional, and to satisfy mass conservation and  
273 Newton's second law. The flow is also assumed to  
274 be lossless everywhere except at the glottal opening.  
275 This main glottal flow (volume velocity) component  
276 is described by

$$\dot{U}(t) = \frac{1}{I_L} (p_s(t) - R_g(t)U(t)), \quad (6)$$

277 where  $p_s(t)$  is the driving stagnation pressure at the  
278 lungs whose time variation is assumed to be slow,  $I_L$   
279 regulates the inertia of the load air column, and  $R_g(t)$   
280 represents non-recoverable losses in the glottis.

281 Equation (6) is related to Newton's second law for  
282 the air column in motion, and it can be derived (fol-  
283 lowing [31, Section 2.2]) from the pressure balance  
284  $p_s = p_g + p_a$ , where the pressure change from the  
285 lungs to the outside space is the sum of the glottal  
286 pressure loss  $p_g$  and the accelerating pressure  $p_a$  of  
287 the fluid column in the airways. To obtain an expres-  
288 sion for  $p_a$ , the power of accelerating an (incompress-  
289 ible) fluid column is considered. This power is equal  
290 to the derivative of the kinetic energy of the fluid col-  
291 umn, yielding  $p_a(t)U(t) = \rho U(t)\dot{U}(t) \int \frac{d\vec{r}}{A(\vec{r})^2}$ , where  
292 the integration is extended over the VT and SGT vol-  
293 umes. Here,  $A(\vec{r})$  denotes the area of the fluid column  
294 cross-section that contains the position vector  $\vec{r}$ , and  
295 incompressibility  $A(\vec{r})v(\vec{r}, t) = U(t)$  was used. By de-  
296 noting the nominal value of inertance  $I_L = \rho \int \frac{d\vec{r}}{A(\vec{r})^2}$ ,  
297 these equations yield  $p_a = I_L \dot{U}(t)$ . In the context  
298 of the airways, the nominal inertance can be split  
299 into VT and SGT contributions  $I_V = \rho \int_0^{L_{VT}} \frac{ds}{A(s)}$  and  
300  $I_S = \rho \int_0^{L_S} \frac{ds}{A_S(s)}$ , respectively, so that  $I_L = I_V + I_S$ ;  
301 see Sections 2.3 and 2.4.

302 Unfortunately, the integration over the volume of  
303 airways (even if the SGT geometry was available) does

not necessarily yield the correct total inertance. The  
flow outside of mouth as well as the masses of the  
lungs, diaphragm, etc., are coupled to the flow. For  
the same reason, the inertial effect for VT and SGT,  
observed in the low frequency limit of the acoustic  
equations (10) and (14), does not give a sufficient ac-  
count of the total intertance since not all of it is due to  
acoustics. Thus, the inertance parameter  $I_L$  must, in  
general, be used as a tuning parameter. The high fre-  
quency feedback from the VT acoustics to the glottal  
flow, a particularly notable effect in phonations where  
the glottis does not fully close, is not included in (6).

The glottal pressure loss consists of two components  
following [40]

$$p_g = R_g(t)U(t) = \frac{12\mu L_g U(t)}{h H_L(t)^3} + \frac{k_g \rho U(t)^2}{2h^2 H_L(t)^2}. \quad (7)$$

The first term represents the viscous pressure loss,  
and it is motivated by the Hagen–Poiseuille law in a  
narrow aperture. It approximates the pressure loss in  
the glottis using a rectangular tube of width  $h$ , height  
 $H_L$ , and length  $L_g$ . The parameter  $\mu$  is the kinematic  
viscosity of air. The second term takes into account  
the pressure losses not attributable to viscosity in the  
same sense as the first. The coefficient  $k_g$  represents  
the difference between pressure drop at the glottal  
inlet and recovery at the outlet. This coefficient de-  
pends not only on the glottal geometry but also on the  
glottal opening, driving pressure, and flow through  
the glottis [41]. Equations (6)–(7) bear resemblance  
to the description of airflow in [12, 13] where the pres-  
sure drop, loss, and recovery effects, however, are ac-  
counted for by flow separation in a diverging channel.

The pressure  $p(x, t)$  in the glottis is given in terms  
of  $U = U(t)$  by making use of the Bernoulli theo-  
rem  $p(x, t) + \frac{1}{2}\rho V(x, t)^2 = p_s$  for the Venturi effect,  
where  $V(x, t)$  is the velocity within the glottis, and the  
mass conservation law  $hH(x, t)V(x, t) = U(t)$ . Since  
each vocal fold has two degrees of freedom,  $p(x, t)$  and  
the VT/SGT counter pressure  $p_c$  can be reduced to  
an aerodynamic force pair  $F_A = [F_{A,1} \ F_{A,2}]^T$  where  
 $F_{A,1}$  acts at  $x = L$  and  $F_{A,2}$  at  $x = 0$  in Figure 1  
(bottom). This reduction can be carried out by using  
the total force and moment balance equations

$$\begin{aligned} F_{A,1} + F_{A,2} &= h \int_0^L (p(x, t) - p_r) dx \quad \text{and} \\ LF_{A,1} &= \frac{h}{\cos^2 \phi} \int_0^L x(p(x, t) - p_r) dx - LA_{pc} p_c, \end{aligned} \quad (8)$$

where  $\phi = \phi(t)$  is the angle of the inclined vocal fold  
surface as shown in Figure 1 (top),  $A_{pc}$  accounts for  
the moment arms and areas on which  $p_c$  acts (see  
equation (16)), and  $p_r$  is the reference pressure cor-  
responding to the equilibrium position  $w_{ij} = 0$  for  
 $i, j = 1, 2$ . Since the displacements  $w_{ij}$  are in the  $y$ -  
direction only, the aerodynamic forces have been as-  
sumed to act in this direction as well. The moment is

evaluated with respect to point  $(x, y) = (0, 0)$  for the lower fold and  $(x, y) = (0, H_0)$  for the upper fold.

The force calculations are done using the pressure difference  $p(x, t) - p_r$  so that  $F_{A,1}$  and  $F_{A,2}$  vanish when  $p(x, t) = p_r$  and  $p_c = 0$ . The reference pressure is associated with the hydrostatic pressure reference level in vibrating tissues, and it is expected to satisfy  $p_r \leq p_s$ . If  $p_r = p_s$  is used, the aerodynamic force always tries to close the glottis. For small flow velocities  $V(x, t)$ , using  $p_r < p_s$  results in the driving pressure  $p_s$  pushing the vocal folds open more strongly than the aerodynamic force pulls them close. There is no obvious way to determine the true magnitude of  $p_r$  as it is an outcome of dynamic pressure equalisation processes related to  $p_s$  and the additional partial pressure due to haemodynamics in tissues. For this work, it is assumed that  $p_r = 0.5p_s^0$ , where  $p_s^0 = p_s(0)$ , and the equilibrium gap parameter  $g_L > 0$  so that starting simulations with a closed glottis is not necessary.

Evaluation of the integrals in (8) yields, for  $H_L > 0$ ,

$$\begin{aligned}
 F_{A,1} &= \frac{hL}{2 \cos^2 \phi} \left( -\frac{\rho U^2}{h^2 H_L (H_0 - H_L)} \right. \\
 &\quad \left. + \frac{\rho U^2}{h^2 (H_L - H_0)^2} \ln \left( \frac{H_0}{H_L} \right) + (p_s - p_r) \right) \\
 &\quad - A_{pc} p_c, \quad \text{and} \\
 F_{A,2} &= \frac{hL}{2 \cos^2 \phi} \left( \frac{\rho U^2 (H_0 \sin^2 \phi + H_L \cos^2 \phi)}{h^2 H_L H_0 (H_0 - H_L)} \right. \\
 &\quad \left. - \frac{\rho U^2}{h^2 (H_L - H_0)^2} \ln \left( \frac{H_0}{H_L} \right) + \cos(2\phi) (p_s - p_r) \right) \\
 &\quad + A_{pc} p_c.
 \end{aligned} \tag{9}$$

During the glottal closed phase (i.e., when  $H_L(t) < 0$ ), the aerodynamic force (9) is not enabled, and the vocal fold load force is instead given by equation (5).

## 2.3 Vocal Tract Acoustics

A generalised version of Webster's horn model resonator is used as acoustic loads to represent both the VT and the SGT. It is given by

$$\frac{A(s)}{c^2 \Sigma(s)^2} \frac{\partial^2 \psi}{\partial t^2} + 2\pi\alpha W(s) \frac{\partial \psi}{\partial t} - \frac{\partial}{\partial s} \left( A(s) \frac{\partial \psi}{\partial s} \right) = 0, \tag{10}$$

where  $c$  denotes the speed of sound, the parameter  $\alpha \geq 0$  regulates the energy dissipation through air/tissue interface, and the solution  $\psi = \psi(s, t)$  is the velocity potential of the acoustic field; i.e.,  $v = -\frac{\partial \psi}{\partial s}$ .

Then the sound pressure is given by  $p = \rho \frac{\partial \psi}{\partial t}$ , where  $\rho$  denotes the density of air. The generalised Webster's model for acoustic waveguides has been derived from the wave equation in a tubular domain in [42], its solvability and energy notions have been treated in [43], and the approximation properties in [44].

The generalised Webster's equation (10) is applicable if the VT is approximated as a curved

tube of varying cross-sectional area and length  $L_{VT}$ . The three-dimensional centreline  $\gamma(s)$  of the tube is parametrised using distance  $s \in [0, L_{VT}]$  from the superior end of the glottis. At every  $s$ , the cross-sectional area of the tube perpendicular to the centreline is given by the area function  $A(s)$ , and the (hydrodynamic) radius of the tube, denoted by  $R(s)$ , is defined by  $A(s) = \pi R(s)^2$ . The curvature of the tube is  $\kappa(s) = \|\gamma''(s)\|$ , and the curvature ratio  $\eta(s) = R(s)\kappa(s) < 1$ .

The final parameters appearing in (10) are the stretching factor  $W(s)$  and the sound speed correction factor  $\Sigma(s)$  for curvature, defined by

$$\begin{aligned}
 W(s) &= R(s) \sqrt{R'(s)^2 + (\eta(s) - 1)^2}, \quad \text{and} \\
 \Sigma(s) &= \left( 1 + \frac{1}{4} \eta(s)^2 \right)^{-1/2}.
 \end{aligned} \tag{11}$$

### 2.3.1 Boundary conditions

The VT resonator is coupled to the glottal flow given by equation (6) with

$$\frac{\partial \psi}{\partial s}(0, t) = -\frac{U_{AC}(t)}{A(0)}, \tag{12}$$

where the DC component has been removed from the glottal flow, i.e.,  $U_{AC}(t) = U(t) - \frac{1}{T} \int_{t-T}^t U(\tau) d\tau$  with  $T = 2/f_0$ . The effect of this removal is negligible when phonation has become stable, but it is more pronounced at the beginning of simulations when a stable waveform has not yet developed. Equations (10)–(12) characterise a variant of the source-filter model in the sense that the acoustics of the VT is only excited at the glottis.

At the lips, the reactive acoustic response of the exterior space is modelled by the differential equation

$$\begin{aligned}
 &-R_m L_m \frac{\partial \psi}{\partial s}(L_{VT}, t) \\
 &= \frac{\rho}{A(L_{VT})} \left( R_m \psi(L_{VT}, t) + L_m \frac{\partial \psi}{\partial s}(L_{VT}, t) \right),
 \end{aligned} \tag{13}$$

which corresponds to the impedance  $Z(\xi) = \frac{\xi R_m L_m}{R_m + \xi L_m}$  of the same form as the ‘‘first-order high pass model’’ for termination of an acoustic horn in [45, Section 4.1]. The circuit topology of this model is the parallel coupling of a resistor and an inductor.

## 2.4 Subglottal acoustics

Anatomically, the SGT consists of the airways below the larynx: trachea, bronchi, bronchioles, alveolar ducts, alveolar sacs, and alveoli. This system has been modelled either as a tree-like structure [27] or, more simply, as an acoustic horn whose area increases towards the lungs [34, 46]. We take the latter approach and denote the cross-sectional area and the horn radius by  $A_S(s)$  and  $R_S(s)$  (see equation (17)),

433 respectively, where  $s \in [0, L_S]$  and  $L_S$  is the nominal  
434 length of the SGT.

435 Since the subglottal horn is assumed to be  
436 straight, we have  $\eta = 0$ ,  $\Sigma = 1$  and  $W_s(s) =$   
437  $R_S(s)\sqrt{R'_S(s)^2 + 1}$ . Then equations (10)–(12) trans-  
438 late to

$$\begin{cases} \frac{A_S(s)}{c^2} \frac{\partial^2 \tilde{\psi}}{\partial t^2} + 2\pi\alpha W_s(s) \frac{\partial \tilde{\psi}}{\partial t} - \frac{\partial}{\partial s} \left( A_S(s) \frac{\partial \tilde{\psi}}{\partial s} \right) = 0, \\ \frac{\partial \tilde{\psi}}{\partial t}(L_S, t) + \theta_s c \frac{\partial \tilde{\psi}}{\partial s}(L_S, t) = 0, \\ \frac{\partial \tilde{\psi}}{\partial s}(0, t) = \frac{U_{AC}(t)}{A_S(0)}, \end{cases} \quad (14)$$

439 where the solution  $\tilde{\psi}$  is the velocity potential for the  
440 SGT acoustics. Instead of using the reactive bound-  
441 ary dynamics (13), the termination loss at lungs is  
442 characterised by normalised acoustic resistance  $\theta_s \geq 0$   
443 in equation (14). SGT acoustics is an important factor  
444 in phonation in general but its contribution to changes  
445 occurring during glide simulations is negligible as long  
446 as  $f_o$  is far from the subglottal resonances.

## 447 2.5 Acoustic counter pressure

448 The feedback coupling from VT/SGT acoustics back  
449 to vocal fold surfaces is realised as the product of the  
450 acoustic counter pressure  $p_c = p_c(t)$  and the moment  
451 corrected area  $A_{pc} = A_{pc}(t)$  as already shown in equa-  
452 tions (5) and (9) above.

453 The counter pressure is the resultant of VT and  
454 SGT pressure components, and it is given in terms of  
455 velocity potentials from equations (10) and (14) by

$$p_c(t) = Q_{pc}\rho \left( \psi_t(0, t) - \tilde{\psi}_t(0, t) \right), \quad (15)$$

456 where tuning parameter  $Q_{pc} \in [0, 1]$  enables scaling  
457 the magnitude of the feedback. The parameter  $Q_{pc}$  is  
458 necessary because the wedge geometry tends to over-  
459 estimate the area of the vocal fold surface on which  
460  $p_c$  can do work, and further, it is difficult to directly  
461 estimate the proportions of the underlying flow and  
462 the superimposed acoustics. In simulations, overesti-  
463 mation of the acoustic feedback forces leads to perma-  
464 nently non-stationary, even chaotic vibrations of the  
465 vocal folds, which are outside the scope of this work.

466 The area  $A_{pc}$  is best understood in reference to the  
467 moment balance in equation (8), although it appears  
468 in the same way in both equations (5) and (9). For  
469 each vocal fold,  $p_c$  acts on the area  $\frac{1}{2}(H_V - H_L)h$  and  
470 produces a moment arm of  $\frac{1}{4}(2H_0 - H_V - H_L)$  around  
471 points  $(x, y) = (0, 0)$  and  $(x, y) = (0, H_0)$  for the lower  
472 and upper folds, respectively. Hence

$$A_{pc} = \frac{h}{8L}(H_V - H_L)(2H_0 - H_V - H_L). \quad (16)$$

473 Equations (15) and (16) assume that both the VT  
474 and SGT pressure components act in the  $x$ -direction  
475 only (i.e., horizontally in Figure 1 (top)). This as-  
476 sumption minimises the tendency of the wedge geom-  
477 etry to overestimate the effect of the SGT compared  
478 to the effect of the VT.

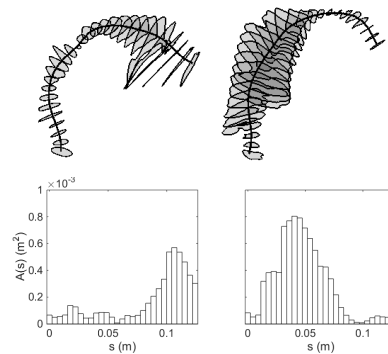


Figure 2: Top: The VT intersections extracted during phonation of [a] and [i]. Bottom: The resulting area functions for equation (10) as a function of distance from the glottis.

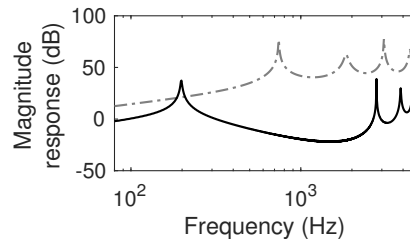


Figure 3: The magnitude responses of the VT acoustic loads obtained by simulating output for an impulse input for [a] (dashed gray) and [i] (solid black). The response of [a] has been raised by 50 dB for clarity.

## 479 3 Parameters

### 480 3.1 Vocal tract

Table 1: VT parameter values.

Parameter	[a]	[i]
Inertance, $I_V$	2540 $\frac{\text{kg}}{\text{m}^4}$	2820 $\frac{\text{kg}}{\text{m}^4}$
Length, $L_{VT}$	132 mm	136 mm
1 <sup>st</sup> resonance, $f_{R1}$	742 Hz	198 Hz
2 <sup>nd</sup> resonance, $f_{R2}$	1846 Hz	2791 Hz
Area at mouth	299 mm <sup>2</sup>	66 mm <sup>2</sup>
$R_m$	$1.98 \cdot 10^6 \frac{\text{kg}}{\text{s m}^4}$	$8.96 \cdot 10^4 \frac{\text{kg}}{\text{s m}^4}$
$L_m$	$33.2 \frac{\text{kg}}{\text{m}^4}$	$70.6 \frac{\text{kg}}{\text{m}^4}$
$\text{Re}(Z(400\pi i))$	879	$4.44 \cdot 10^4$
$\text{Im}(Z(400\pi i))$	$4.17 \cdot 10^4$	$4.48 \cdot 10^4$

481 Solving Webster’s equation requires that the VT is  
482 represented with an area function and a centreline,  
483 from which curvature information can be computed.  
484 Two different VT geometries corresponding to vowel-  
485 s from a healthy 26 years old female are used: A  
486 prolonged [a] produced at  $f_o = 168$  Hz and similarly  
487 produced [i] at  $f_o = 210$  Hz. These geometries have  
488 been obtained by MRI using the experimental setting  
489 described in [47]; see also [48, 49, 50] for earlier ap-

490 proaches. The extraction of the computational geom-  
 491 etry from raw MRI data has been carried out by the  
 492 custom software described in [51, 52]. The VT geom-  
 493 etries and their area functions are shown in Figure 2,  
 494 their simulated frequency responses in Figure 3, and  
 495 and the VT geometry dependent parameter values are  
 496 given in Table 1.

497 The reactive acoustic loading (13) at the lips re-  
 498 quires values for  $R_m$  and  $L_m$ . The values in Table 1  
 499 were obtained by interpolation at 200 Hz from the  
 500 piston model given in [53, Chapter 7, Eq. (7.4.31)]  
 501 and tuning of  $R_m$  to remove excessive fluctuations in  
 502 simulated waveforms. The low order rational model  
 503  $Z(\xi) = \frac{\xi R_m L_m}{R_m + \xi L_m}$  approximates the irrational piston  
 504 model impedance very well for frequencies within  
 505 100 Hz . . . 2 kHz, and the frequency responses in Fig-  
 506 ure 3 are reasonable as well.

### 507 3.2 Subglottal tract

508 Full SGT geometry cannot be constructed from the  
 509 MRI data that is used for the VT. Instead, an ex-  
 510 ponential horn is used as the SGT area function for  
 511 equation (14)

$$A_S(s) = A_S(0)e^{\epsilon s}, \text{ where } \epsilon = \frac{1}{L_S} \ln \left( \frac{A_S(L_S)}{A_S(0)} \right) \quad (17)$$

512 following [46]. The values for  $A_S(0) = 2 \text{ cm}^2$  and  
 513  $A_S(L_S) = 10 \text{ cm}^2$  are taken from [46, Figure 1]. The  
 514 horn length  $L_S$  is selected so that the lowest subglot-  
 515 tal resonance is  $f'_{R1} = 500 \text{ Hz}$  which results in the  
 516 second lowest resonance at  $f'_{R2} = 1.0 \text{ kHz}$ . This is a  
 517 reasonable value for  $f_{R1}$  based on [9, Table 1]; see also  
 518 [39, 54, 55] and [27, Figure 1]. The SGT lung termi-  
 519 nation resistance in equation (14) is given the value  
 520  $\theta_s = 1$  which corresponds to an absorbing boundary  
 521 condition. The air column in this SGT model has a  
 522 inertia parameter value  $I_S = 1040 \text{ kg/m}^4$ .

### 523 3.3 Static parameter values

524 Table 2 lists the numerical values of physiological and  
 525 physical constants used in all simulations. Note that  
 526 the vocal fold springs are, for this study, placed sym-  
 527 metrically about the midpoint of the vocal folds.

528 The masses in  $M$  are calculated by combining the  
 529 vocal fold shape function used in [32] with female vo-  
 530 cal fold length reported in [56], yielding a total vi-  
 531 brating mass  $m_1 + m_2 + m_3 = 0.27 \text{ g}$ . A first estimate  
 532 for the spring coefficients in  $K$  is calculated by as-  
 533 suming that the first eigenfrequency of the vocal folds  
 534 matches the starting frequency for the simulations.  
 535 The spring coefficients are then adjusted until simu-  
 536 lations produce  $f_o \approx 145 \text{ Hz}$ , giving the initial  $K^0$   
 537 for equations (18)–(19) with total spring coefficients  
 538  $k_1 + k_2 = 248 \text{ N/m}$ . For details of these calculations,  
 539 see [31] and [30].

540 The vocal fold damping parameter  $\beta$  plays an im-  
 541 portant but problematic role in vocal fold models.

Table 2: Physical and physiological constants.

Parameter	Value
speed of sound in air, $c$	343 $\frac{\text{m}}{\text{s}}$
density of air, $\rho$	1.2 $\frac{\text{kg}}{\text{m}^3}$
kinematic viscosity of air, $\mu$	18.27 $\frac{\mu\text{N}\cdot\text{s}}{\text{m}^2}$
VT/SGT loss coeff., $\alpha$	76 $\frac{\mu\text{s}}{\text{m}}$
glottal gap at rest at $x = 0$ , $g_0$	10.9 mm
glottal gap at rest at $x = L$ , $g_L$	0.4 mm
control gap above glottis, $H_V$	2 mm
vocal fold length [56], $h$	10 mm
vocal fold thickness [32], $L$	6.8 mm
1 <sup>st</sup> vocal fold spring location, $l_1$	0.85
2 <sup>st</sup> vocal fold spring location, $l_2$	0.15
contact spring constant [32], $k_H$	730 $\frac{\text{N}}{\text{m}^{3/2}}$
viscous thickness, $L_g$	1.5 mm
SGT length, $L_S$	350 mm
resistance at lungs, $\theta_s$	1
entrance/exit coeff., $k_g$	0.6
initial driving pressure, $p_s^0$	650 Pa

If there is too much damping, sustained oscillations  
 do not occur. Conversely, too low damping causes  
 instability in simulated vocal fold oscillations. The  
 magnitude of physically realistic damping in vibrat-  
 ing tissues is not available, and, due to its simpli-  
 fications, the present model could fail to produce  
 quasi-stationary phonation even if realistic experi-  
 mental damping values were used. For this article,  
 $\beta = 0.009 \text{ kg/s}$  is used as it produces slowly changing  
 glottal pulse amplitudes when simulations are carried  
 out with constants parameters as well as in feedback  
 free glides. This damping is small enough that the  
 resonances of the mass-spring-damper system (1) are  
 defined approximately by  $M$  and  $K$  alone.

In this work, the nominal values of  $I_V$  and  $I_S$ , given  
 in Table 1 and Section 3.2, are used without tuning.

## 548 4 Computational Aspects

### 549 4.1 Production of pitch glides

The  $f_o$ -glides are simulated by controlling two param-  
 eter values dynamically. First, the matrix  $K$  is scaled  
 while keeping the matrix  $M$  constant as the relative  
 magnitudes of  $M$  and  $K$  essentially determine the re-  
 sonance frequencies of vocal fold model (1). This ap-  
 proach is based on the assumption that the vibrating  
 mass and the length of the vocal folds are not signif-  
 icantly changed when the speaker's pitch increases; a  
 reasonable simplification as far as the frequency range  
 is small and register changes are excluded.

The driving pressure  $p_s$  is the second parameter  
 used to control the glide. The dependence of  $f_o$  on  
 $p_s$  has been observed in simulations [8, 57], physical  
 experiments using upscaled replicas [12], as well as in  
 humans [58] and excised canine larynges [59]. The

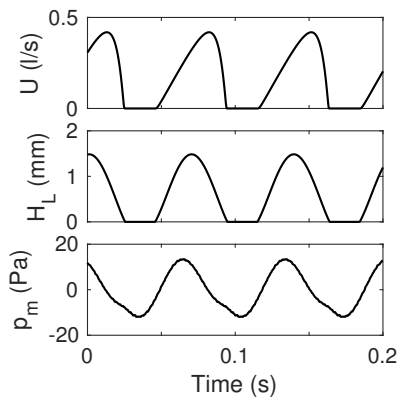


Figure 4: Simulated pulse shapes for [i] with feedback ( $Q_{pc} = 0.1$ ) before the glide begins: glottal flow  $U$ , glottal gap  $H_L$ , and sound pressure at the lips  $p_m$ .

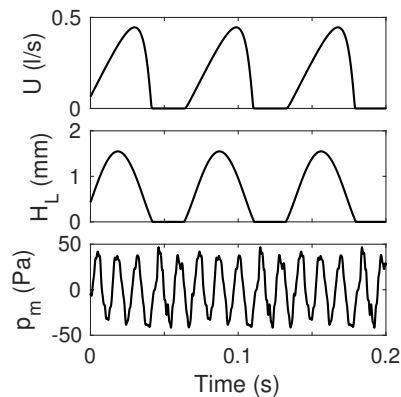


Figure 5: Simulated pulse shapes for [a] with feedback ( $Q_{pc} = 0.1$ ) before glide: glottal flow  $U$ , glottal gap  $H_L$ , and sound pressure at the lips  $p_m$ .

575 impact of  $p_s$  on  $f_o$  is, however, secondary in these  
 576 glides (the  $f_o$  trajectories with and without  $p_s$  control  
 577 differ by at most 10%). Instead,  $p_s$  is scaled in order  
 578 to maintain phonation and to prevent large changes  
 579 in phonation type as the stiffness of the vocal folds  
 580 changes. It was found by trial and error, that equal  
 581 scaling of  $p_s$  and  $K$  best maintained the glottal open  
 582 quotient  $OQ$  (proportion of glottal cycle during which  
 583 the glottis is open, see [60, Figure 4]), the closing  
 584 quotient  $CIQ$  (proportion of the glottal cycle during  
 585 which the flow is decreasing), and the maximum of  
 586  $H_L$  approximately steady over the upward glide when  
 587 acoustic feedback was disabled.

588 The parameters are scaled exponentially with time

$$K(t) = 2.2^{2t/T} K^0, \quad p_s(t) = 2.2^{t/T} p_s^0 \quad (18)$$

589 for rising glides, and

$$K(t) = 2.2^{2-2t/T} K^0, \quad p_s(t) = 2.2^{1-t/T} p_s^0 \quad (19)$$

590 for falling glides. The duration of the glide is  $T = 3$  s,  
 591 and  $t$  is the time from the beginning of the glide. Note  
 592 that the temporal scale of the glides is long compared  
 593 to glottal cycles, and hence the control parameters  $K$   
 594 and  $p_s$  can be regarded as static from the point of view  
 595 of the vocal fold dynamics. Other starting conditions  
 596 (particularly, vocal fold displacements and velocities,  
 597 and pressure and velocity distributions in the resonators)  
 598 are taken from stabilised simulations. These parameters  
 599 produce glides with  $f_o$  approximately in the range  
 600 [145 Hz, 315 Hz], although the exact range  
 601 depends on the VT geometry and feedback level.

## 602 4.2 Numerical realisation

603 The model equations are solved numerically using  
 604 MATLAB software and custom-made code. The vocal  
 605 fold equations of motion (1) are solved by the fourth  
 606 order Runge–Kutta time discretisation scheme. The  
 607 flow equation (6) is solved by the backward Euler  
 608 method. The VT and SGT are discretised by

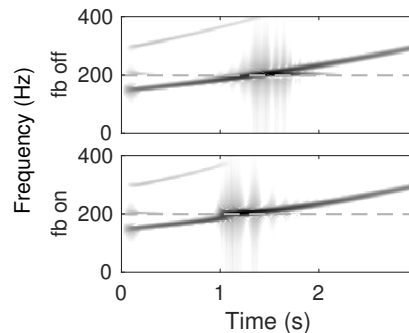


Figure 6: Spectrogram of pressure at lips during glide for [i]. Top: without feedback ( $Q_{pc} = 0$ ). Bottom: with feedback ( $Q_{pc} = 0.1$ ). Dashed gray line is  $f_{R1}$ .

609 FEM using piecewise linear elements ( $N = 29$  for  
 610 VT and  $N = 10$  for SGT) and the physical energy  
 611 norm of Webster’s equation. Energy preserving  
 612 Crank–Nicolson time discretisation (i.e., Tustin’s  
 613 method [61]) is used for the resonators. The time  
 614 step is generally  $10 \mu\text{s}$  which is small enough to keep  
 615 the frequency warping in Tustin’s method under one  
 616 semitone for frequencies under 13 kHz. Reduced time  
 617 step, however, is used near glottal closure. This is  
 618 due to the discontinuity in the aerodynamic force (9)  
 619 at the closure which requires numerical treatment by  
 620 interpolation and time step reduction as explained in  
 621 [31, Section 2.4.1].

622 Solving the equations of motion of the vocal folds  
 623 is the computationally most expensive part of the  
 624 model, taking approximately 55% of the running time  
 625 in simulations of steady phonation with constant  
 626 parameter values. In comparison, solving the Web-  
 627 ster’s equations with precomputed mass, stiffness, and  
 628 damping matrices takes approximately 10% of the  
 629 simulation time, and the flow equation solver less than  
 630 2%. Simulation of 1 s takes approximately 20 s on a  
 631 standard professional desktop computer.



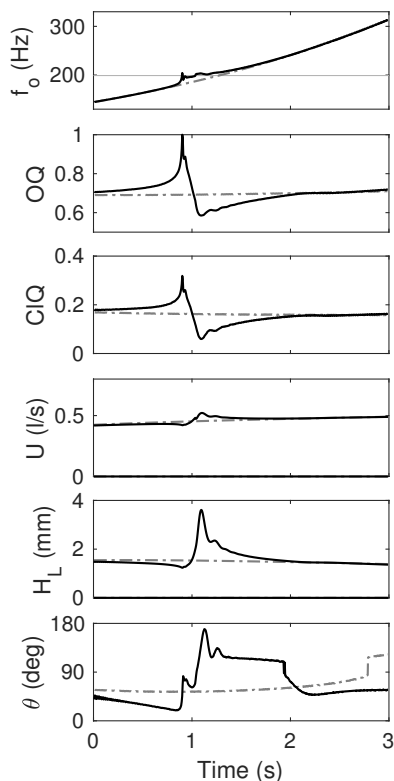


Figure 7: Glide for [i] with feedback ( $Q_{pc} = 0.1$ ) (solid black) and without feedback ( $Q_{pc} = 0$ ) (dashed gray). Shown are fundamental frequency  $f_o$  (horizontal gray line is  $f_{R1}$ ), open quotient  $OQ$ , closing quotient  $ClQ$ , envelopes of glottal flow  $U$  and gap  $H_L$ , and phase difference  $\theta$  between  $m_{j1}$  and  $m_{j2}$ .

## 5 Simulation Results

The glottal flow  $U$  and gap  $H_L$  (or more generally the glottal area  $hH_L$ ) pulses produced by the model (Figures 4–5) appear realistic when compared to the experimental data presented in [54, Figures 4–7], the signals produced by different numerical models (see [8, Figures 14a–14c], [27, Figures 10–11], [39, Figures 8 and 10], [62, Figure 6], [63, Figure 5]), and the glottal pulse waveforms obtained by inverse filtering in, e.g., [64, Figures 10–13], [60, Figures 3 and 6], and [65, Figures 5.3, 5.4, and 5.17]. Quantitative comparison of the model to the LF model can be found in [66]. The skewing of  $U$  relative to  $H_L$  – an effect that has been observed in natural speech, e.g., with the help of inverse filtering in [67, 68] – is mainly produced by the inertial term in (6).

The results of upward glide simulations for [i] are shown in Figures 6–7. Figure 6 displays spectrograms of the sound pressure signal at the lips with and without feedback. For Figure 7, the  $f_o$  trajectory,  $OQ$ , and  $ClQ$  have been extracted from  $U$  pulse by pulse. Envelopes of  $U$ , and  $H_L$  are also displayed, and the phase difference  $\theta$  between  $m_{j1}$  and  $m_{j2}$  has been es-

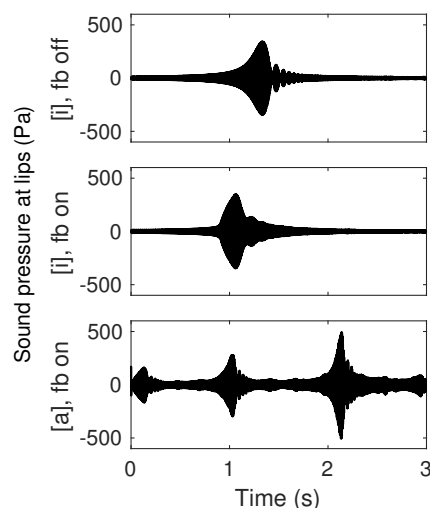


Figure 8: Sound pressures at the lips during upward glides. Top: [i] without feedback ( $Q_{pc} = 0$ ). Middle: [i] with feedback ( $Q_{pc} = 0.1$ ). Bottom: [a] with feedback ( $Q_{pc} = 0.1$ ).

timated based on how much peaks in  $H_0$  are delayed compared to  $H_L$ .

The simulations indicate a consistent locking pattern in  $f_o$  trajectories at  $f_{R1}[i]$  which vanishes if the VT feedback is decoupled by setting  $Q_{pc} = 0$ . This locking pattern for rising glides can be seen in Figure 6 as a discontinuity in the  $f_o$  contour near  $f_{R1}$  followed by an interval where  $f_o$  appears to be approximately constant. More details are visible in the  $f_o$  trajectory in Figure 7: a rapid rise in  $f_o$  (hereafter referred to as a jump), a locking to a plateau at approximately  $f_{R1}$ , and a smooth release. The height of the jump, degree of overshoot and oscillations about the plateau level, as well as the duration of the locking event depend on parameter choices (see, e.g., Figure 11). In the glide displayed in Figure 7, the  $f_o$  trajectories deviate by over 1% in the range 178–215 Hz as measured from feedback free trajectory, and the overshoot at the frequency jump reaches 205 Hz. The flattest part of the locking, which follows the overshoot, occurs at 195–197 Hz.

The frequency jump in the simulations is preceded by a decrease in vocal fold oscillation and glottal flow amplitudes (Figure 7), and a decrease in the phase difference between upper and lower vocal fold masses. This is accompanied by increased breathiness in the phonation, as characterised by increasing  $OQ$  and  $ClQ$  values, which reduces the effect of the feedback from the acoustics to the vocal folds. The locking plateau coincides with a nearly constant rate of decreasing  $OQ$  and  $ClQ$ , and increasing amplitude of, in particular,  $H_L$ . At the same time, there are large but smooth changes in  $\theta$ . After the release of  $f_o$  the glottal pulse characteristics return gradually to the feedback free trajectories, except for  $\theta$ . The sudden

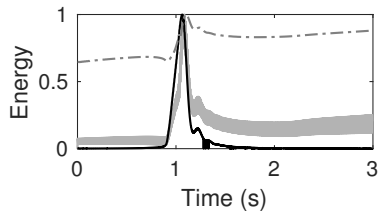


Figure 9: Normalised envelope of energy in VT acoustics (solid black) and in the glottal flow  $U$  (dashed gray), and energy in vocal fold vibrations (solid gray) in upward glide for [i] with  $Q_{pc} = 0.1$ .

690 changes in  $\theta$  seen at 1.9 s with feedback and at 2.8 s  
 691 without feedback are caused by the method of esti-  
 692 mating  $\theta$ . Near these instants  $H_0$  pulses have shallow  
 693 double peaks, and the sudden change occurs when  
 694 the dominant peak shifts from one to the other. Note,  
 695 however, that changes in pulse shapes are smooth near  
 696 these instants. Further,  $H_0$  and  $H_L$  have well defined  
 697 single peaks at and near the locking event, so changes  
 698 in  $\theta$  there are not caused by this same phenomenon.

699 This locking behaviour of  $f_o$  or the related wave-  
 700 form changes are not observed for glides of [a] where  
 701  $f_{R1}[a]$  is not inside the simulated frequency range  
 702 [145 Hz, 315 Hz]. The differences in the  $f_o$  trajec-  
 703 tories and glottal pulse characteristics between feedback  
 704 ( $Q_{pc} = 0.1$ ) and feedback free ( $Q_{pc} = 0$ ) confi-  
 705 gurations are negligible for [a].

706 The VT resonance  $f_{R1}[i]$  and the resonance frac-  
 707 tions  $f_{R1}[a]/5 = 148$  Hz,  $f_{R1}[a]/4 = 186$  Hz and  
 708  $f_{R1}[a]/3 = 247$  Hz are within the frequency range,  
 709 and the corresponding events are visible in the sound  
 710 pressure signal at the lips (Figure 8). Note that de-  
 711 spite this visibility, corresponding events can be seen  
 712 in the glottis only for the event in the middle panel,  
 713 i.e.  $f_{R1}[i]$  with feedback. For [a], the pressure sig-  
 714 nals with and without feedback are nearly identical (only  
 715 glide with feedback is shown in Figure 8). For [i], the  
 716 largest difference in the pressures is the timing of the  
 717 resonance event.

718 When feedback is disabled, energy cannot be trans-  
 719 ferred from the resonating vocal tract to the oscillat-  
 720 ing vocal folds or to the glottal flow. Figure 9 shows  
 721 how energy, normalised to one, in each of the subsys-  
 722 tems develops when feedback is on. As the resonance  
 723 nears,  $p_c$  does work on the vocal folds increasing the  
 724 energy in the vocal fold oscillations which in turn feeds  
 725 energy into  $U$ . Since  $p_c$  has an increasingly strong pe-  
 726 riodic component at  $f_{R1}[i]$ , all three subsystems get  
 727 locked to this frequency. Unlocking occurs when the  
 728 first vocal fold eigenfrequency has been raised suffi-  
 729 ciently for the energy in the oscillations to win out  
 730 over the frequency of  $p_c$ .

731 Rising and falling glides show different perturba-  
 732 tion patterns as shown in Figure 10. The  $x$ -axis in  
 733 this figure is the relative vocal fold stiffness, which for  
 734 rising glides is  $2.2^{t/T}$  and for falling glides  $2.2^{1-t/T}$

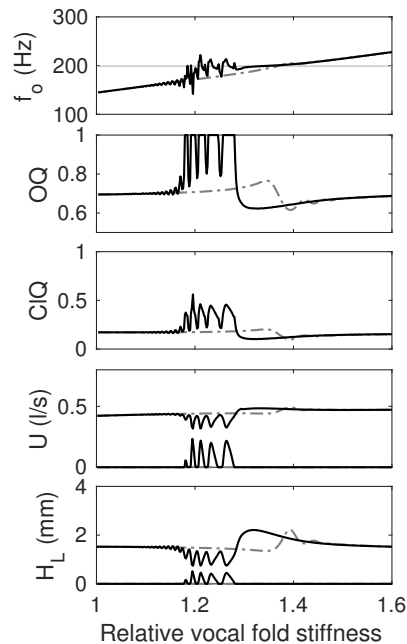


Figure 10: Upward (dashed gray) and downward (solid black) glides for vowel [i] with  $Q_{pc} = 0.04$ . Shown are fundamental frequency  $f_o$  ( $f_{R1}$  indicated by horizontal gray line), open quotient  $OQ$ , closing quotient  $ClQ$ , and the envelopes of glottal flow  $U$  and gap  $H_L$ . On the  $x$ -axis, relative vocal fold stiffness refers to the coefficient of the  $K^0$  matrix in equations (18) and (19).

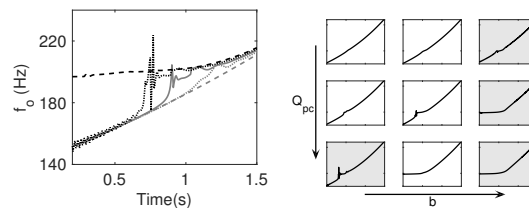


Figure 11: Left:  $f_o$  trajectories for [i] with different values of  $Q_{pc}$ : gray dashed 0.0, gray dotted 0.05, gray solid 0.1, black dotted 0.15, and black dashed 0.2. Right:  $f_o$  trajectories for [i] qualitatively as  $Q_{pc}$  and  $\beta$  increase in the direction of the arrow. Light gray background indicates that small parameter changes can lead to loss of quasi-stable glides.

735 as given in equations (18) and (19). For given model  
 736 parameter values, falling glides exhibit more fluctua-  
 737 tions in glottal pulse parameters at the locking event  
 738 and the perturbation lasts longer. The fluctuations in  
 739  $f_o$  in the falling glides during the locking and at fre-  
 740 quencies below this are qualitatively similar to what  
 741 occurs at extreme values of  $Q_{pc}$  and  $\beta$  for rising glides.

742 The feedback parameter  $Q_{pc}$  plays, unsurprisingly,  
 743 a key role in the  $f_o$  jump and locking in glides for  
 744 [i] as shown in Figure 11 (left). With no acoustic  
 745 feedback to the vocal folds, there are no perturbations

in  $f_o$ , whereas with a high  $Q_{pc}$ , starting a glide with  $f_o$  below  $f_{R1}$  is not possible without decreasing  $K^0$ . If a starting  $f_o$  below  $f_{R1}$  is obtainable, a high  $Q_{pc}$  value results in a large overshoot at the jump, and fluctuations in  $f_o$  both before the jump and at the beginning of the plateau.

Besides  $Q_{pc}$ , the locking pattern is also sensitive to other model parameters, in particular the vocal fold damping  $\beta$ . In fact,  $\beta$  and  $Q_{pc}$  affect the locking behaviour in complementary ways, as qualitatively shown in Figure 11 (right). The full frequency range [145 Hz, 315 Hz] for  $f_o$  can be obtained with modal locking if  $Q_{pc} \in [0.05, 0.12]$  and  $\beta \in [0.005, 0.015]$ . Beyond these ranges, an increase in one parameter needs to be compensated for with a decrease in the other. Otherwise, the locking pattern disappears or the simulated  $f_o$  range is reduced to above  $f_{R1}[i]$ .

The stability of glide simulations (understood as slowly changing amplitude envelope of glottal flow  $U$ ) becomes a serious issue at high values of one or both of the parameters  $Q_{pc}$  and  $\beta$ . The driving pressure  $p_s$  in glide simulations is dynamically controlled as given in equations (18)–(19). If  $p_s$  were instead kept constant, we would observe an increasing  $OQ$  and decreasing amplitudes of glottal flow and vocal fold oscillations throughout the glide but the qualitative behaviour of modal locking events, including the behaviour of phonation type parameters around these events, would remain very similar.

## 6 Discussion

We have reported observations on the locking of  $f_o$  at a resonance of the VT in simulated pitch glides. The locking behaviour shows a consistent time-dependent behaviour that is similar for rising and falling glides. The  $f_o$  jump at the beginning of the locking in rising glides and end of the locking in falling glides occurs together with and increased breathiness of phonation as characterised by open quotient  $OQ$  and closing quotient  $ClQ$ . During the locking plateau, these parameters indicated an approximately steady decrease in breathiness.

The locking takes place only at frequencies determined by supraglottal resonances. Use of  $p_s$  as a secondary control parameter for the glides ensure that the main cause for changes in  $OQ$  and  $ClQ$  is the acoustic loading. By modifying the strength of the acoustic feedback (i.e., the parameter  $Q_{pc}$  in equation (15)) and vocal fold tissue losses (i.e., the parameter  $\beta$ ), the locking tendency at  $f_{R1}[i]$  may be modulated from non-existent (where both  $Q_{pc}$  and  $\beta$  have low values) to extreme locking at  $f_{R1}[i]$  without release (where  $Q_{pc}$  and/or  $\beta$  have large values); see Figure 11. Small changes to the model (as discussed below) leave the locking behaviour at  $f_{R1}[i]$  unchanged, even though the model parameter values required for the desired glottal waveform change (cf.

[28, 29]). We conclude that the simulation results on vowel glides reported in Section 5 reflect the model behaviour in a consistent and robust manner.

To what extent do the simulation results validate the proposed model? The model produces perturbations of the glottal pulses at VT resonances and, additionally, sound pressure perturbations at some of the VT resonance fractions. Of the former, a wide existing literature was reviewed in Section 1. Observations on perturbations in speech at formant fractions have not been reported, to our knowledge, in experimental literature. There is a particular temporal pattern of locking in simulated perturbations at  $f_{R1}[i]$  as shown in Figures 6 and 7 (topmost panel). A similar pattern can be seen in the speech spectrograms given in [17, Figure 5], [16, Figure 4], as well as in the vowel glide samples in the data set of [3]. The pitch trajectory and speech spectrogram in [19, Figure 4] also show locking but no release. A similar locking behaviour can also be interpreted to lie behind the experimental results shown in [12, Figures 10b and 13b], and it also tends to emerge in model simulations even if the acoustic feedback is realised in different manner; see, e.g., [14, Figures 13 and 14] and [69, Figure 6].

### 6.1 Acoustics

The effect of physically realistic values of parameter  $\alpha$  in model simulations is negligible; see [25, Section 5] and [30, Section 3.3.2]. These losses move the VT resonance positions computed from equations (10) slightly. On the other hand, the VT resonances are quite sensitive to the parameters of the parallel RL model in equation (13), similar to the simplified model proposed in [45, Eq. (28)]. In its most general form, the model in [45, Eq. (39)] is an integro-differential delay equation with nine parameters and a single delay lag. Unfortunately, it cannot be introduced to Webster’s model as a boundary condition: this is the salient feature of equation (13) that simplifies the implementation of the FEM solver.

It is expected that the otherwise small subglottal effect in simulations will get more pronounced when  $f_o \rightarrow f'_{R1}$ , and similarly VT impact for [a] will increase when  $f_o \rightarrow f_{R1}[a]$ . These resonance frequencies, as well as the fractions  $f_{R1}[i]/n$ ,  $n = 2, 3, \dots$ , are not included in the glides because the two glide controls appear to be insufficient to maintain phonation through such a large frequency range. Such glides would likely require dynamic control of vocal fold length and mass as well. The similarity of the VT and SGT resonators is visible near the resonance fractions in the presented glides, however: The first subglottal resonance fraction  $f'_{R1}/2$  shows up in the counter pressure (15) in the same way as  $f_{R1}[a]/n$ .

The SGT acoustics model proposed in [27] is likely to produce the correct resonance distribution and frequency-dependent energy dissipation rate at the

lung end without tuning. The horn model requires tuning of the horn geometry in order to get the lowest subglottal resonance realistic  $f'_{R1} = 500$  Hz. Doing so freezes all the higher subglottal resonances at fixed positions, e.g.,  $f'_{R2} = 1.0$  kHz. The branching subglottal models given in [27, Figure 8] have the second subglottal resonance between 1.3 kHz and 1.5 kHz. It was observed in [70] that the soft tissues introduce an additional nonacoustic resonance to the subglottal system that is lower than the first subglottal formant  $f'_{R1}$  attributed to air column dynamics. There is no obvious way how a horn model could be used to accommodate such a resonance at ca. 350 Hz due to the yielding wall dynamics.

## 6.2 Vocal folds and glottal flow

The vocal fold geometry shown in Figure 1 (top) leads to a simple expression for the aerodynamic force in equation (9). The further simplification of keeping the direction of  $p(x, t)$  constant (i.e., considering changes in  $\phi$  negligible) is possible without affecting the qualitative behaviour of the model. The difference between the driving pressure  $p_s$  and the reference pressure  $p_r$  can be included in the force balance when the glottis is closed (equation (5)) although the wedge-shaped vocal folds, their point-like collision, and the assumption of incompressible glottal flow lead to overestimation of the effect. This addition causes an increase in the open quotient throughout simulations, but if the model parameters are adjusted to achieve a phonation similar to Figures 4–5 before the glides, the locking behaviour remains qualitatively unchanged.

Replacing the sharp peaks by flat tops in Figure 1 results in phonation that has typically lower open quotient (OQ) compared to the original wedge-like geometry. This change makes it easier to adjust the parametrisation of the model to obtain some phonation targets. In particular, the value of the glottal loss parameter  $k_g$  can then be based on experimental values (e.g., [41]) since the model geometry becomes more similar to the experimental model geometry (M5).

The importance of entrance and exit effects represented by  $k_g$  can be seen, for example, by comparing simulated volume velocities and glottal areas with the experimental curves in [40, Figure 3], obtained from a physical model of the glottis. In model simulations, leaving out this transglottal pressure loss term changes the glottal pulse waveform significantly if other model parameters are kept the same, as shown in [30, Figure 3.7]. About half of the total pressure loss in simulations is due to entrance and exit effects at the peak of opening of the glottis; see [30, Figure 3.6]. However, the behaviour of the simulated  $f_o$  trajectories over  $f_{R1}[i]$  does not change if  $k_g = 0$ . Then, however, the vowel glide must be produced by different model parameter values.

The glottal flow has been studied extensively since 1950's. Compared to the flow model used here, physiologically more faithful glottal flow solvers have been proposed in, e.g., [35, 46, 62, 71, 72] and [73]. As pointed out in [72], more sophisticated flow models are challenging to couple to acoustic resonators since the interface between the flow-mechanical (in particular, the turbulent) and the acoustic components is no longer clearly defined.

Direct feedback from VT acoustics to the glottal flow can be added to the model although it has been left outside the scope of this work. In implementing this feedback mode, particular care must be taken to remove the additional acoustic contribution in the inertial effect, which is already accounted for by (6). The impact of this feedback mechanism is expected to be notable around the  $f_o$  jump, when the glottal closure is short or non-existent.

Turbulence in supraglottal space is a spatially distributed acoustic source, and it does not provide a spatially localised acoustic signal for the resonator in equation (12). Much of the turbulence noise energy lies above 4 kHz where Webster's model equation (10) is not an accurate description [74, 75]. The unmodelled supraglottal jet may even exert an additional aerodynamic force to vocal folds that would not be part of the acoustic counter pressure  $p_c$ .

## 7 Conclusions

We have presented a model for vowel production, based on (partial) differential equations, that consists of submodels for glottal flow, vocal folds oscillations, and acoustic responses of the VT and SGT cavities. The model was used for simulations of rising and falling vowel glides of [a, i] in frequencies that span one octave [145 Hz, 315 Hz]. This interval contains the lowest VT resonance  $f_{R1}$  of [i] but not that of [a]. Perturbation events in simulated vowel glides were observed at VT acoustic resonances, or at some of their fractions but nowhere else.

The fundamental frequency  $f_o$  of the simulated vowel was observed to lock to  $f_{R1}[i]$  but similar locking was not seen at any of the resonance fractions of [a]. The locking events were accompanied by changes in the phonation: increased breathiness below and partially at the locking frequency and steady change in breathiness during most of the lock. If these changes can also be detected in glides produced by human speakers, e.g., by using electroglottography, they may provide an indirect means of identifying locking events when coincidence of  $f_o$  and  $f_{R1}$  makes it challenging to track them both.

The locking event takes place only when the acoustic feedback from VT to vocal folds is present, and then it has a characteristic time-dependent behaviour. A large number of simulation experiments were carried out with different parameter settings of the model

970 to verify the robustness and consistency of all observa-  
 971 tions. The similarity between simulated pitch pattern  
 972 and experimental results in literature was achieved  
 973 by using feedback from acoustics to vocal fold tis-  
 974 sues, indicating that this feedback mode can be strong  
 975 enough to affect speech outcomes.

976 The simulation model does not include the neural  
 977 control actions on the vocal fold structures or dy-  
 978 namic modifications of the VT geometry. There is  
 979 also a significant control action affecting the driving  
 980 stagnation pressure and it has been used as a control  
 981 variable in equations (18)–(19) for glide productions.  
 982 In humans, neural control actions are part of feedback  
 983 loops, of which some are auditive, and some others op-  
 984 erate directly through tissue innervation and the cen-  
 985 tral nervous system. So little is known about these  
 986 feedback mechanisms that their explicit mathematical  
 987 modelling seems infeasible. Instead, the model  
 988 parameters for simulations are tuned so that the sim-  
 989 ulated glottal pulse waveform corresponds to experi-  
 990 mental speech data. Despite these simplifications the  
 991 model appears to be sufficiently detailed to replicate  
 992 the observations found in literature.

## 993 Acknowledgements

994 This study was funded by the Academy of Finland  
 995 (projects no. 284671 and 312490), the Finnish gradu-  
 996 ate school in engineering mechanics, Finnish Academy  
 997 project Lastu 135005, 128204, and 125940; European  
 998 Union grant Simple4All (grant no. 287678), Aalto  
 999 Starting Grant 915587, and Åbo Akademi Institute  
 1000 of Mathematics. The authors would like to thank the  
 1001 four anonymous reviewers in 2013 and 2016 for com-  
 1002 ments leading to many improvements of the model.

## 1003 References

- 1004 [1] T. Chiba, M. Kajiyama: The vowel, its nature and  
 1005 structure. Phonetic Society of Japan, Tokyo, 1941.
- 1006 [2] G. Fant: Acoustic theory of speech production. Mou-  
 1007 ton, The Hague, 1960.
- 1008 [3] D. Aalto, J. Malinen, M. Vainio, Modal locking be-  
 1009 tween vocal fold and vocal tract oscillations: Ex-  
 1010 periments and statistical analysis. ArXiv e-prints,  
 1011 arXiv:1211.4788, 2016.
- 1012 [4] I. R. Titze, R. J. Baken, K. W. Bozeman,  
 1013 S. Granqvist, N. Henrich, C. T. Herbst, D. M.  
 1014 Howard, E. J. Hunter, D. Kaelin, R. D. Kent,  
 1015 J. Kreiman, M. Kob, A. Löfqvist, S. McCoy, D. G.  
 1016 Miller, H. Noé, R. C. Scherer, J. R. Smith, B. H.  
 1017 Story, J. G. Švec, S. Ternström, J. Wolfe: Toward a  
 1018 consensus on symbolic notation of harmonics, reso-  
 1019 nances, and formants in vocalization. The Journal of  
 1020 the Acoustical Society of America **137** (2015) 3005–  
 1021 3007.
- 1022 [5] P. Alku, J. Horáček, M. Airas, F. Griffond-Boitier,  
 1023 A.-M. Laukkanen: Performance of glottal inverse fil-  
 1024 tering as tested by aeroelastic modelling of phona-  
 1025 tion and FE modelling of vocal tract. Acta Acustica  
 1026 united with Acustica **92** (2006) 717–724.
- [6] P. Alku, J. Pohjalainen, M. Vainio, A.-M. Laukka-  
 1027 nen, B. H. Story: Formant frequency estimation of  
 1028 high-pitched vowels using weighted linear prediction.  
 1029 The Journal of the Acoustical Society of America **134**  
 1030 (2013) 1295–1313.
- [7] J. Guðnason, D. D. Mehta, T. F. Quatieri: Eval-  
 1032 uation of speech inverse filtering techniques using  
 1033 a physiologically based synthesizer. Proceedings of  
 1034 2015 IEEE International Conference on Acoustics,  
 1035 Speech and Signal (ICASSP), April 2015, 4245–4249.
- [8] K. Ishizaka, J. L. Flanagan: Synthesis of voiced  
 1037 sounds from a two mass model of the vocal cords.  
 1038 Bell System Technical Journal **51** (1972) 1233–1268.
- [9] S. F. Austin, I. R. Titze: The effect of subglottal  
 1040 resonance upon vocal fold vibration. Journal of Voice  
 1041 **11** (1997) 391–402.
- [10] Z. Zhang, J. Neubauer, D. A. Berry: The influence of  
 1043 subglottal acoustics on laboratory models of phona-  
 1044 tion. The Journal of the Acoustical Society of Amer-  
 1045 ica **120** (2006) 1558–1569.
- [11] J. C. Lucero, K. G. Lourenço, N. Hermant, A. Van  
 1047 Hirtum, X. Pelorson: Effect of source-tract acoustical  
 1048 coupling on the oscillation onset of the vocal folds.  
 1049 The Journal of the Acoustical Society of America **132**  
 1050 (2012) 403–411.
- [12] N. Rutu, X. Pelorson, A. Van Hirtum, I. Lopez-  
 1052 Arteaga, A. Hirschberg: An in-vitro setup to test  
 1053 the relevance and the accuracy of low-order vocal  
 1054 folds models. The Journal of the Acoustical Society  
 1055 of America **121** (2007) 479–490.
- [13] N. Rutu, X. Pelorson, A. Van Hirtum: Influence  
 1057 of acoustic waveguides lengths on self-sustained os-  
 1058 cillations: Theoretical prediction and experimental  
 1059 validation. The Journal of the Acoustical Society of  
 1060 America **123** (2008) 3121–3121.
- [14] I. R. Titze: Nonlinear source-filter coupling in phona-  
 1062 tion: Theory. The Journal of the Acoustical Society  
 1063 of America **123** (2008) 2733–2749.
- [15] H. Hatzikirou, W. T. Fitch, H. Herzel: Voice instabil-  
 1065 ities due to source-tract interactions. Acta Acustica  
 1066 united with Acustica **92** (2006) 468–475.
- [16] I. T. Tokuda, M. Zemke, M. Kob, H. Herzel: Biome-  
 1068chanical modeling of register transitions and the role  
 1069 of vocal tract resonators. The Journal of the Acous-  
 1070 tical Society of America **127** (2010) 1528–1536.
- [17] I. R. Titze, T. Riede, P. Popolo: Nonlinear source-  
 1072 filter coupling in phonation: Vocal exercises. The  
 1073 Journal of the Acoustical Society of America **123**  
 1074 (2008) 1902–1915.
- [18] M. Zaňartu, D. D. Mehta, J. C. Ho, G. R. Wodicka,  
 1076 R. E. Hillman: Observation and analysis of in vivo  
 1077 vocal fold tissue instabilities produced by nonlinear  
 1078 source-filter coupling: A case study. The Journal of  
 1079 the Acoustical Society of America **129** (2011) 326–  
 1080 339.

- 1082 [19] L. Wade, N. Hanna, J. Smith, J. Wolfe: The role of vocal tract and subglottal resonances in producing vocal instabilities. *The Journal of the Acoustical Society of America* **141** (2017) 1546–1559. 1140
- 1083 1141
- 1084 1142
- 1085
- 1086 [20] K. L. Kelly, C. C. Lochbaum: Speech synthesis. Proceedings of the Fourth International Congress on Acoustics, 1962, Paper G42, 1–4. 1143
- 1087 1144
- 1088 1145
- 1089 [21] H. K. Dunn: The calculation of vowel resonances, and an electrical vocal tract. *The Journal of the Acoustical Society of America* **22** (1950) 740–753. 1146
- 1090 1147
- 1091 1148
- 1092 [22] S. El-Masri, X. Pelorson, P. Saguet, P. Badin: Development of the transmission line matrix method in acoustics. Applications to higher modes in the vocal tract and other complex ducts. *International Journal of Numerical Modelling: Electronic Networks, Devices and Fields* **11** (1998) 133–151. 1149
- 1093 1150
- 1094 1151
- 1095 1152
- 1096 [23] J. Mullen, D. Howard, D. Murphy: Waveguide physical modeling of vocal tract acoustics: Flexible formant bandwidth control from increased model dimensionality. *IEEE Transactions on Audio, Speech, and Language Processing* **14** (2006) 964–971. 1153
- 1097 1154
- 1098 1155
- 1099 1156
- 1100 [24] S. Rienstra, A. Hirschberg: An introduction to acoustics. Eindhoven University of Technology, 2013. 1157
- 1101 1158
- 1102 1159
- 1103 [25] K. van den Doel U. M. Ascher: Real-time numerical solution of Webster’s equation on a nonuniform grid. *IEEE Transactions on Audio, Speech, and Language Processing* **16** (2008) 1163–1172. 1160
- 1104 1161
- 1105 1162
- 1106 1163
- 1107 1164
- 1108 [26] J. Horáček, V. Uruba, V. Radolf, J. Veselý, V. Bula: Airflow visualization in a model of human glottis near the self-oscillating vocal folds model. *Applied and Computational Mechanics* **5** (2011) 21–28. 1165
- 1109 1166
- 1110 1167
- 1111 1168
- 1112 [27] J. C. Ho, M. Zaňartu, G. R. Wodicka: An anatomically based, time-domain acoustic model of the subglottal system for speech production. *The Journal of the Acoustical Society of America* **129** (2011) 1531–1547. 1169
- 1113 1170
- 1114 1171
- 1115 1172
- 1116 1173
- 1117 [28] T. Murtola, J. Malinen: Waveform patterns in pitch glides near a vocal tract resonance. Proceedings of INTERSPEECH 2017, Stockholm, 2017, 3487–3491. 1174
- 1118 1175
- 1119 1176
- 1120 1177
- 1121 [29] A. Aalto, T. Murtola, J. Malinen, D. Aalto, M. Vainio: Modal locking between vocal fold and vocal tract oscillations: Simulations in time domain. ArXiv e-prints, arXiv:1506.01395, 2017. 1178
- 1122 1179
- 1123 1180
- 1124 [30] T. Murtola: Modelling vowel production. Licentiate thesis, Aalto University School of Science, Espoo, Finland, 2014. 1181
- 1125 1182
- 1126 1183
- 1127 [31] A. Aalto: A low-order glottis model with nonturbulent flow and mechanically coupled acoustic load. Master’s thesis, Helsinki University of Technology, Espoo, Finland, 2009. 1184
- 1128 1185
- 1129 1186
- 1130 1187
- 1131 [32] J. Horáček, P. Šidlof, J. G. Švec: Numerical simulation of self-oscillations of human vocal folds with Hertz model of impact forces. *Journal of Fluids and Structures* **20** (2005) 853–869. 1188
- 1132 1189
- 1133 1190
- 1134 1191
- 1135 [33] J. Liljencrants: A translating and rotating mass model of the vocal folds. *STL-QPSR* **32** (1991) 1–18. 1192
- 1136 1193
- 1137 [34] N. J. C. Lous, G. C. J. Hofmans, R. N. J. Veldhuis, A. Hirschberg: A symmetrical two-mass vocal-fold model coupled to vocal tract and trachea, with application to prosthesis design. *Acta Acustica united with Acustica* **84** (1998) 1135–1150. 1194
- 1138 1195
- 1139 [35] X. Pelorson, A. Hirschberg, R. R. van Hassel, A. P. J. Wijnands, Y. Auregan: Theoretical and experimental study of quasisteady-flow separation within the glottis during phonation. Application to a modified two-mass model. *The Journal of the Acoustical Society of America* **96** (1994) 3416–3431. 1196
- 1197 1197
- 1198 [36] B. H. Story, I. R. Titze: Voice simulation with a body-cover model of the vocal folds. *The Journal of the Acoustical Society of America* **97** (1995) 1249–1260. 1198
- 1199 1199
- 1200 [37] B. D. Erath, M. Zaňartu, K. C. Stewart, M. W. Plesniak, D. E. Sommer, S. D. Peterson: A review of lumped-element models of voiced speech. *Speech Communication* **55** (2013) 667–690. 1199
- 1201 1200
- 1202 [38] P. Birkholz: A survey of self-oscillating lumped-element models of the vocal folds. In: B. J. Kröger, P. Birkholz, eds., *Studentexte zur Sprachkommunikation: Elektronische Sprachsignalverarbeitung*, 2011, 47–58. 1201
- 1203 1202
- 1204 [39] M. Zaňartu, L. Mongeau, G. R. Wodicka: Influence of acoustic loading on an effective single mass model of the vocal folds. *The Journal of the Acoustical Society of America* **121** (2007) 1119–1129. 1203
- 1205 1204
- 1206 [40] J. van den Berg, J. T. Zantema, P. Doornenbal: On the air resistance and the Bernoulli effect of the human larynx. *Journal of the Acoustical Society of America* **29** (1957) 626–631. 1205
- 1207 1206
- 1208 [41] L. P. Fulcher, R. C. Scherer, T. Powell: Pressure distributions in a static physical model of the uniform glottis: Entrance and exit coefficients. *The Journal of the Acoustical Society of America* **129** (2011) 1548–1553. 1207
- 1209 1208
- 1210 [42] T. Lukkari, J. Malinen: Webster’s equation with curvature and dissipation. ArXiv e-prints, arXiv:1204.4075, 2013. 1209
- 1211 1210
- 1212 [43] A. Aalto, T. Lukkari, J. Malinen: Acoustic wave guides as infinite-dimensional dynamical systems. *ESAIM: Control, Optimisation and Calculus of Variations* **21** (2015) 324–347. 1211
- 1213 1212
- 1214 [44] T. Lukkari, J. Malinen: A posteriori error estimates for Webster’s equation in wave propagation. *Journal of Mathematical Analysis and Applications* **427** (2015) 941–961. 1213
- 1215 1214
- 1216 [45] T. Hélie, X. Rodet: Radiation of a pulsating portion of a sphere: application to horn radiation. *Acta Acustica united with Acustica* **89** (2003) 565–577. 1215
- 1217 1216
- 1218 [46] P. Birkholz, D. Jackel, B. Kröger: Simulation of losses due to turbulence in the time-varying vocal system. *IEEE Transactions on Audio, Speech, and Language Processing* **15** (2007) 1218–1226. 1217
- 1219 1218
- 1220 [47] D. Aalto, O. Aaltonen, R.-P. Happonen, P. Jääsaari, A. Kivelä, J. Kuortti, J.-M. Luukinen, J. Malinen, T. Murtola, R. Parkkola, J. Saunavaara, T. Soukka, M. Vainio: Large scale data acquisition of simultaneous MRI and speech. *Applied Acoustics* **83** (2014) 64–75. 1219
- 1221 1220
- 1222 1221
- 1223 1222
- 1224 1223
- 1225 1224
- 1226 1225
- 1227 1226
- 1228 1227
- 1229 1228
- 1230 1229
- 1231 1230
- 1232 1231
- 1233 1232
- 1234 1233
- 1235 1234
- 1236 1235
- 1237 1236
- 1238 1237
- 1239 1238

- 1199 [48] B. Story, I. Titze, E. Hoffman: Vocal tract area func- 1258  
1200 tions from magnetic resonance imaging. *The Journal* 1259  
1201 *of the Acoustical Society of America* **100** (1996) 537– 1260  
1202 554.
- 1203 [49] B. H. Story, I. R. Titze, E. A. Hoffman: Vocal tract 1261  
1204 area functions for an adult female speaker based on 1262  
1205 volumetric imaging. *The Journal of the Acoustical* 1263  
1206 *Society of America* **104** (1998) 471–487. 1264
- 1207 [50] B. H. Story, I. R. Titze: Parameterization of vocal 1265  
1208 tract area functions by empirical orthogonal modes. 1266  
1209 *Journal of Phonetics* **26** (1998) 223–260. 1267
- 1210 [51] A. Kivelä: Acoustics of the Vocal Tract: MR image 1268  
1211 segmentation for modelling. Master’s thesis, Aalto 1269  
1212 University School of Science, Espoo, Finland, 2015.
- 1213 [52] A. Ojalampi, J. Malinen: Automated segmentation 1270  
1214 of upper airways from MRI: Vocal tract geometry 1271  
1215 extraction. *Proceedings of BIOIMAGING 2017*, 2017, 1272  
1216 77–84. 1273
- 1217 [53] P. M. Morse, K. U. Ingard: *Theoretical acoustics*. 1274  
1218 McGraw-Hill, 1968. 1275
- 1219 [54] B. Cranen, L. Boves: Pressure measurements dur- 1276  
1220 ing speech production using semiconductor miniature 1277  
1221 pressure transducers: Impact on models for speech 1278  
1222 production. *The Journal of the Acoustical Society of* 1279  
1223 *America* **77** (1985) 1543–1551. 1280
- 1224 [55] B. Cranen, L. Boves: On subglottal formant analysis. 1281  
1225 *The Journal of the Acoustical Society of America* **81** 1282  
1226 (1987) 734–746.
- 1227 [56] I. R. Titze: Physiologic and acoustic differences be- 1283  
1228 tween male and female voices. *The Journal of the* 1284  
1229 *Acoustical Society of America* **85** (1989) 1699–1707. 1285
- 1230 [57] D. Scimarella, C. d’Alessandro: On the acoustic sen- 1286  
1231 sitivity of a symmetric two-mass model of the vo- 1287  
1232 cal folds to the variation of control parameters. *Acta* 1288  
1233 *Acustica united with Acustica* **90** (2004) 746–761. 1289
- 1234 [58] P. Lieberman, R. Knudson, J. Mead: Determination 1290  
1235 of the rate of change of fundamental frequency with 1291  
1236 respect to subglottal air pressure during sustained 1292  
1237 phonation. *The Journal of the Acoustical Society of* 1293  
1238 *America* **45** (1969) 1537–1543. 1294
- 1239 [59] I. R. Titze: On the relation between subglottal pres- 1295  
1240 sure and fundamental frequency in phonation. *The* 1296  
1241 *Journal of the Acoustical Society of America* **85** 1297  
1242 (1989) 901–906. 1298
- 1243 [60] P. Alku: Glottal inverse filtering analysis of human 1299  
1244 voice production - a review of estimation and param- 1300  
1245 eterization methods of the glottal excitation and their 1301  
1246 applications. *Sadhana* **36** (2011) 623–650. 1302
- 1247 [61] V. Havu, J. Malinen: The Cayley transform as a time 1303  
1248 discretization scheme. *Numerical Functional Analysis* 1304  
1249 *and Optimization* **28** (2007) 825–851. 1305
- 1250 [62] I. R. Titze: Regulating glottal airflow in phonation: 1306  
1251 Application of the maximum power transfer theorem 1307  
1252 to a low dimensional phonation model. *The Journal* 1308  
1253 *of the Acoustical Society of America* **111** (2002) 367– 1309  
1254 376.
- 1255 [63] I. R. Titze: Parameterization of the glottal area, glot- 1310  
1256 tal flow, and vocal fold contact area. *The Journal of* 1311  
1257 *the Acoustical Society of America* **75** (1984) 570–580.
- [64] P. Alku: Glottal wave analysis with pitch syn- 1258  
1259 chronous iterative adaptive inverse filtering. *Speech* 1260  
1261 *Communication* **11** (1992) 109–118. 1262
- [65] H. Pulakka: Analysis of human voice production us- 1263  
1264 ing inverse filtering, high-speed imaging, and elec- 1264  
1265 troglottography. Master’s thesis, Helsinki University 1266  
1266 of Technology, Espoo, Finland, 2005. 1267
- [66] A. Aalto, P. Alku, J. Malinen: A LF-pulse from 1268  
1269 a simple glottal flow model. *Proceedings of the* 1270  
1271 *6th International Workshop on Models and Analy-* 1271  
1272 *sis of Vocal Emissions for Biomedical Applications* 1272  
1273 *(MAVEBA2009)*, Florence, 2009, 199–202. 1273
- [67] M. Berouti, D. Childers, A. Paige: Glottal area ver- 1274  
1275 sus glottal volume-velocity. *IEEE International Con-* 1275  
1276 *ference on Acoustics, Speech, and Signal Processing* 1276  
1277 *ICASSP ’77 (1977)* **2** 33–36. 1277
- [68] S. Granqvist, S. Hertegård, H. Larsson, J. Sund- 1278  
1279 berg: Simultaneous analysis of vocal fold vibration 1279  
1280 and transglottal airflow: exploring a new experimen- 1280  
1281 tal setup. *Journal of Voice* **17** (2003) 319–330. 1281
- [69] N. Ruty, X. Pelorson, A. van Hirtum: Influence of 1282  
1283 acoustic waveguides lengths on self-sustained oscilla- 1282  
1284 tions: Theoretical prediction and experimental vali- 1283  
1285 dation. *Proceedings of Acoustics ’08*, Paris, June 29- 1284  
1286 July 4, 2008, 1243–1247. 1285
- [70] S. M. Lulich, H. Arsikere: Tracheo-bronchial soft tis- 1286  
1287 sue and cartilage resonances in the subglottal acoustic 1286  
1288 input impedance. *Journal of the Acoustical Society of* 1287  
1289 *America* **137** (2015) 3436–3446. 1288
- [71] B. D. Erath, S. D. Peterson, M. Zaňartu, G. R. Wod- 1289  
1290 icka, M. W. Plesniak: A theoretical model of the pres- 1289  
1291 sure field arising from asymmetric intraglottal flows 1290  
1292 applied to a two-mass model of the vocal folds. *The* 1291  
1293 *Journal of the Acoustical Society of America* **130** 1292  
1294 (2011) 389–403. 1293
- [72] P. Punčochářová-Pořízková, K. Kozel, J. Horáček, 1294  
1295 J. Fürst: Numerical simulation of unsteady compres- 1294  
1296 sible low Mach number flow in a channel. *Engi-* 1295  
1297 *neering Mechanics* **17** (2010) 83–97. 1296
- [73] P. Šidlof, J. Horáček, V. Řidký: Parallel CFD simu- 1297  
1298 lation of flow in a 3D model of vibrating human vocal 1298  
1299 folds. *Computers & Fluids* **80** (2013) 290–300. 1299
- [74] T. Vampola, J. Horáček, A.-M. Laukkanen, J. G. 1300  
1301 Švec: Human vocal tract resonances and the 1301  
1302 corresponding mode shapes investigated by three- 1302  
1303 dimensional finite-element modelling based on CT 1303  
1304 measurement. *Logopedics Phoniatrics Vocology* **40** 1304  
1305 (2013) 1–10. 1305
- [75] T. Vampola, A.-M. Laukkanen, J. Horáček, J. G. 1306  
1307 Švec: Finite element modelling of vocal tract changes 1307  
1308 after voice therapy. *Applied and Computational Me-* 1308  
1309 *chanics* **5** (2011) 77–88. 1309